Highly Dispersed Ruthenium Nanoparticle-Embedded Mesoporous Silica as a Catalyst for the Production of γ-Butyrolactone from Succinic Anhydride

Sang-Ho Chung[1], Hee-Jun Eom[1], Min-Sung Kim[1], Myung Suk Lee[1], and Kwan-Young Lee[1, 2, *]

[1] *Department of Chemical and Biological Engineering, Korea University, 5-1, Anam-dong, Sungbuk-ku,
Seoul 136-701, Republic of Korea*
[2] *Green School, Korea University, 5-1, Anam-dong, Sungbuk-ku, Seoul 136-701, Republic of Korea*

In this study, a novel, strategic method was developed for the synthesis of a mesoporous silica catalyst embedded with ruthenium nanoparticles ($RuNPs/SiO_2$) by combining the polyol and modified sol–gel methods. By applying this new procedure, uniformly synthesized ruthenium nanoparticles with an average size of 3.8 nm and 95% spherical shape were highly dispersed in the mesoporous silica support material. Coordinated carbonyl groups of PVP remaining from the synthesis of the RuNPs were effectively removed by the thermal treatment (calcined at 573 K for 4 h) and the sythesized $RuNPs/SiO_2$ catalysts were reduced under hydrogen at 20 bar for 2 h. These catalysts were analyzed using transmission electron microscopy (TEM), Fourier transform infrared spectroscopy (FT-IR), N_2 adsorption–desorption, and X-ray diffraction (XRD). After the thermal treatment and the reduction procedure, the size and shape of the embedded RuNPs were nearly unchanged, and the catalyst was active in the liquid-phase hydrogenation of succinic anhydride (SAN) to selectively form γ-butyrolactone (GBL) with a maximum yield of 90.1%. This novel catalyst preparation is a potentially useful method for the synthesis of metal nanoparticles as heterogeneous catalysts.

Keywords: Ruthenium Nanoparticle-Embedded Catalysts, Succinic Anhydride, Hydrogenation.

1. INTRODUCTION

In the field of heterogeneous catalysis, several researchers have reported that the activity of a catalyst can be enhanced by loading the active metal as a nanoparticle onto support materials because the ratio of surface atoms to total metal atoms increases when utilizing metal nanoparticles.[1,2] Therefore, much effort recently has been directed towards the preparation and use of nano-sized, noble metal-loaded, heterogeneous catalysts.[3–5] The synthesis of metal nanoparticles is currently an active research area, which spans a variety of approaches including electrochemical reduction,[6] microwave irradiation,[7,8] and the polyol method.[9–13] However, synthesized metal nanoparticles have not been used in heterogeneous catalysis because without support materials, the nano-sized metal particles can aggregate and become deactivated in the reaction conditions or are hard to separate and/or recycle from the reaction mixtures for secondary use.

Recently, several researchers have revealed an effective methods of embedding nanoparticles to create catalysts, which introduce structure-enhancing support materials via a multi-step preparation.[14,15] However, these methods require much effort for the separation of synthesized nanoparticles from the mother liquor,[16] as well as to embed the nanoparticles into the support materials without disturbing the size and shape of the synthesized nanoparticles.

Ruthenium is a well-known noble metal classified in group VIII and is active in various reactions, such as CO oxidation,[14,17] ammonia synthesis,[18] and the Fischer-Tropsch reaction.[19] Ruthenium is also effective in hydrogenation reactions, such as the conversion of fatty acid esters to alcohols,[20] benzene to cyclohexene,[21] and *o*-chloronitrobenzene to *o*-chloroaniline.[22]

In this study, we prepared ruthenium nanoparticle-embedded silica catalysts ($RuNPs/SiO_2$) using a direct embedding procedure, which we applied to the production of γ-butyrolactone (GBL) via liquid-phase hydrogenation of succinic anhydride (SAN). GBL is used for the synthesis of specialty pyrrolidones, such as 2-pyrrolidone and *N*-methyl-2-pyrrolidone. These products can be utilized for pharmaceuticals, extraction solvents, and dielectric materials.[23] For the production of GBL, previous studies have primarily focused on the gas-phase reaction which

---

*Author to whom correspondence should be addressed.
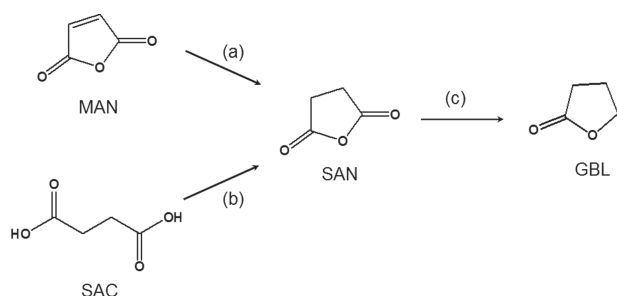
Scheme 1. Production of γ-butyrolactone (GBL) from two different starting materials. MAN: maleic anhydride, SAC: succinic acid, SAN: succinic anhydride.

uses maleic anhydride (MAN) as the starting material (Scheme 1(a)). The MAN-based process is mainly utilized in the petrochemical industry, and it has several drawbacks, such as the continuously rising price of oil and declining oil reservoirs. Consequently, there is growing interest from researchers in biomass conversion for producing fine chemicals such as GBL because of the useful functional groups in the bio-based starting materials.[24] Succinic anhydride can also be produced in solid state using an environmentally benign dehydration process from the well-studied bio-based C4 chemical, succinic acid (SAC)[25] (Scheme 1(b)). Hara et al. studied the liquid-phase hydrogenation of succinic anhydride using the homogeneous catalyst Ru(acac)$_3$, which provided a maximum yield of $\sim 95\%$ of GBL[23] and Herrmann et al. applied a Ru/C catalyst at 513 K to yield GBL in $\sim 85\%$.[26]

This paper describes a method to directly synthesize the RuNPs/SiO$_2$ catalyst, combining the polyol method for the uniformly sized ruthenium nanoparticles and the modified sol–gel method for the mesoporous silica support material. Transmission electron microscopy (TEM), N$_2$ adsorption–desorption analysis, X-ray diffraction (XRD) and Fourier transform infrared spectroscopy (FT-IR) were conducted to analyze the RuNPs/SiO$_2$ catalyst, which exhibited a maximum yield of 90.1% of GBL in the hydrogenation of SAN. Therefore, we expect that this preparation of a RuNPs-embedded catalyst will be an improved method for the preparation of heterogeneous catalysts because it offers advantages in the synthesis of both nanoparticles and their support materials.

2. EXPERIMENTAL DETAILS

The nano-sized ruthenium particles were synthesized by the polyol method in ethylene glycol (HOCH$_2$CH$_2$OH, $\geq 99\%$, reagent plus), which was used as the solvent and reducing agent. The polyvinylpyrrolidone (PVP, CH$_2$CH(NC$_3$H$_6$CO)$_n$, $M_w = 40,000$) was added to the ethylene glycol ([ethylene glycol]/[PVP] = 6067) and fully dissolved by increasing the temperature from 293 K to 323 K over 60 min. Then, the calculated amount of the ruthenium precursor (Ru(acac)$_3$, 97%) was added to

the solution ([Ru]/[PVP] = 10), and the temperature was maintained at 353 K for 20 min with vigorous stirring to fully dissolve the ruthenium precursor. The solution was heated to 453 K with a heating rate of 9 K/min, and the particle formation reaction was conducted for 2 h. The resulting solution of ruthenium nanoparticles (RuNPs) was cooled to room temperature, and then the precursor of siliceous material (SiC$_8$H$_{20}$O$_4$, 98%, reagent grade), anhydrous ethanol (C$_2$H$_5$OH, 99%), ammonium fluoride (NH$_4$F) and DI water were added for the preparation of 3 wt.% RuNPs/SiO$_2$ catalyst by a modified sol–gel method ([TEOS]/[EtOH] = 1 and[H$_2$O]/[NH$_4$F] = 102).[27] The solution was heated to 323 K, leading to gelation within 10 min, and the temperature was maintained for 20 h for the complete gelation of siliceous materials. After the gelation procedure, the gelated RuNPs/SiO$_2$ was filtered and washed with acetone, ethanol, and DI water and dried at 363 K overnight (RuNPs/SiO$_2$-D). Finally, the RuNPs/SiO$_2$-D was calcined at 573 K for 4 h with heating rate of 1 K/min (RuNPs/SiO$_2$-300).

Hydrogenation of succinic anhydride was conducted in a 150 mL high-pressure batch reactor with a magnetic stirrer. The detailed reaction procedure has been previously described.[28] Before the reaction, 0.3 g of the prepared catalyst was reduced under hydrogen gas (ultra high purity, $> 99.999\%$) at 20 bar and 573 K for 2 h (RuNPs/SiO$_2$-300R). After the catalyst reduction, the reaction vessel was charged with 0.5 g of succinic anhydride and 50 mL of 1,4-dioxane. The remaining air was removed by purging the reactor with hydrogen gas, and the pressure was increased to 10 bar with H$_2$. Once the reactor was heated to and maintained the reaction temperature, the pressure was raised to 50 bar with gaseous H$_2$, and the reaction mixture was stirred at 750 rpm for 6 h. To follow the progress of the reaction, approximately 0.3 mL of liquid samples were collected through the sampling line, which was connected to the bottom of reaction vessel. During the sampling procedure, the reaction pressure was maintained by continuously introducing hydrogen gas from the high-pressure gas reservoir.

Samples of the reaction products were analyzed qualitatively, using gas chromatography-mass spectrometry (GC-MS), and quantitatively, using gas chromatography (GC) equipped with a flame ionization detector (FID) and a capillary column (HP-1). The injector temperatures were set at 573 K and the flow rate of helium carrier gas was 1 mL/min (split ratio = 79:1). The oven temperature was programmed at 333 K for 5 min and increased to 503 K with a heating rate of 10 K/min, and the column pressure was 11.5 psi at 313 K and 20.9 psi at 503 K. The FID detector temperature was set at 573 K with flow rates of 30 mL/min for hydrogen and 300 mL/min for high purity air.

Nitrogen adsorption and desorption isotherms were measured at 77 K on an ASAP 2010 analyzer. The RuNPs/SiO$_2$-D sample was pretreated to release any

adsorbed species at 373 K for 2 h, and the other samples (RuNPs/SiO$_2$-300 and RuNPs/SiO$_2$-300R) were pretreated at 473 K for 2 h. The specific area was calculated using the BET (Brunaure–Emmet–Teller) method and the pore sizes of the catalysts were obtained from the desorption branch of nitrogen isotherms using the BJH (Barrett–Joyner–Halenda) method.

X-ray diffraction patterns were recorded on a Rigaku ATX-G diffractometer with Cu Kα radiation ($\lambda = 0.154$ nm) and a step size of 0.01 at a scan rate of 0.1 °/min. An X-ray was generated at 60 kV–300 mA (18 kW) with a rotating Cu-anode source.

Fourier transform infrared spectroscopy data of the synthesized catalysts were recorded with an Infinity Gold FT-IR series spectrometer using the ATR reflection mode at a resolution of 4.0 cm^{-1} for 32 scans.

Transmission electron microscopy images were taken using a Philips FEI Technai G2 F30 machine, operated at 300 kV.

3. RESULTS AND DISCUSSION

The ruthenium nanoparticles (RuNPs) were synthesized by the polyol method, and the TEM image of the RuNPs directly revealed uniformity of their sizes and shapes (Fig. 1). The average size of the RuNPs was 3.8 nm (standard deviation = 0.64 nm) and 95% were spherical. After embedding the RuNPs into SiO$_2$, they were highly dispersed in the silica support material (Fig. 2). After the calcination and reduction of the RuNPs/SiO$_2$-D sample at 573 K, the RuNPs retained their size, but a small portion of the RuNPs sintered when they were in close proximity to each other.
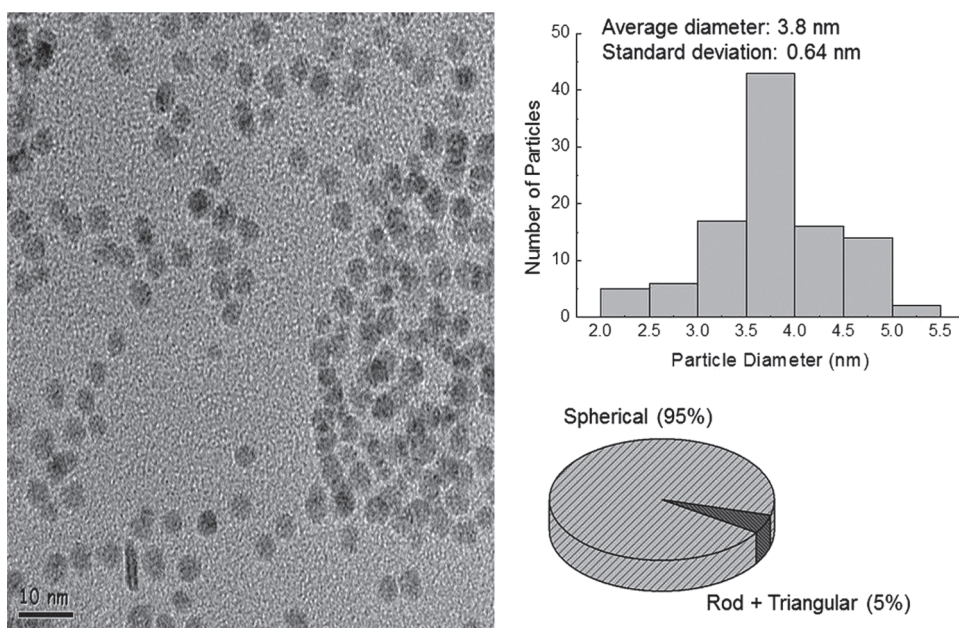
The textural properties of the synthesized RuNPs/SiO$_2$ catalysts are shown in Table I. After the drying procedure, the texture of RuNPs/SiO$_2$-D was not sufficiently developed, but after the calcination at 573 K, the surface area and pore volume significantly increased to 878.6 m^2/g and 0.969 cm^3/g, respectively. These phenomena can be explained by the effective thermal treatment that is needed for the formation of mesoporous silica support when using this modified sol–gel method. After the reduction procedure to prepare RuNPs/SiO$_2$-300R, the surface area and pore volume were maintained without changing the pore size of RuNPs/SiO$_2$-300 even though these properties slightly decreased. Figure 3 shows the nitrogen adsorption–desorption isotherms and the pore-size distributions of the RuNPs/SiO$_2$ catalysts. As shown in Figure 3, all of the catalysts demonstrated the typical type IV isotherms and exhibited H 1 hysteresis loops for the mesoporous materials as a result of capillary condensation.[29, 30] The pore size distributions of the catalysts were obtained from the nitrogen desorption branch by the BJH method (Fig. 3). It was confirmed that the pore structures of the calcined RuNPs/SiO$_2$ catalysts (RuNPs/SiO$_2$-300 and RuNPs/SiO$_2$-300R) were enlarged and this pore-generating phenomena was a result of the thermal treatment.[31–33] Previous studies reported that the formation of pore structures of a size of ∼4 nm resulted from the elimination of PVP, which remained from the synthesis of metal-core and porous silica-shell nanocomposite materials.[31–34]

Figure 4 shows the FT-IR spectrum of pure PVP, RuNPs/SiO$_2$-D, and the calcined RuNPs/SiO$_2$ catalysts (RuNPs/SiO$_2$-300 and RuNPs/SiO$_2$-300R). The broad peaks at ∼3,300 cm^{-1} in the PVP and RuNPs/SiO$_2$-D

Fig. 1. Bright field transmission electron microscopy (BF-TEM) image of synthesized ruthenium nanoparticles (RuNPs). The average particle size, standard deviation, and shape of RuNPs were calculated by counting 100 particles from the TEM images.
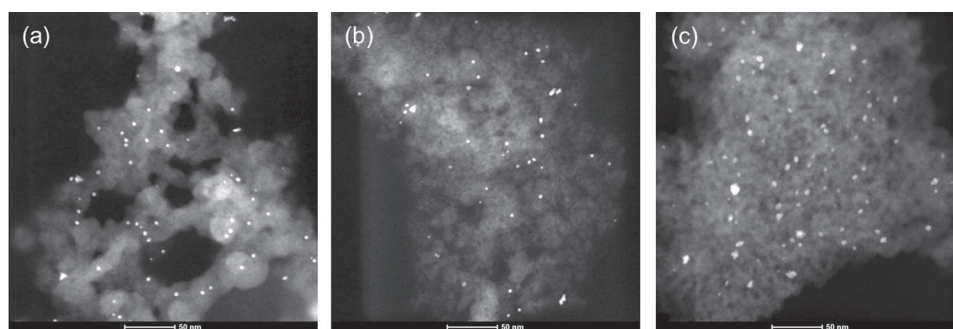
Fig. 2. High-angle annular dark-field scanning transmission electron microscopy (HAADF-STEM) images of RuNPs/SiO$_2$ catalysts. (a) RuNPs/SiO$_2$-D, (b) RuNPs/SiO$_2$-300, and (c) RuNPs/SiO$_2$-300R.

samples were attributed to the stretching bands of hydroxyl groups from adsorbed water, and the peaks at 2960–2850 cm^{-1} and 1289 cm^{-1} were assigned as the stretching modes of the –CH$_2$ and C—N groups of PVP, respectively. In the synthesis of nanoparticles by the polyol method in which PVP was used as stabilizer, the C=O group of PVP was coordinated to the surface metal atoms and prevented the agglomeration and oxidation of the synthesized metal nanoparticles.[34] However, Sanchez et al. observed that the remaining PVP (a stabilizer in nanoparticle synthesis) could cause a decrease in its activity because the carbonyl groups of the PVP can strongly bind to the surface atoms of nanoparticles.[35] After the thermal treatment, the RuNPs/SiO$_2$-300 and RuNPs/SiO$_2$-300R catalysts showed no peaks characteristic of the carbonyl groups of remaining PVP ($\sim$1680 cm^{-1}), which may have been bound to the surface of the RuNPs. This observation is clearly related to the formation of the mesoporous structures of the calcined catalysts.

In Figure 5, the X-ray diffraction patterns of the synthesized RuNPs/SiO$_2$ catalysts are shown. The broad peaks in all of the catalysts at $2\theta = 15°$–$30°$ was due to the amorphous silica, which was used for the support material. In the RuNPs/SiO$_2$-D catalyst, two small peaks appeared at 41.1° and 44.1°, which were assigned to metallic ruthenium with phases of (002) and (011), respectively. After the thermal treatment, the RuNPs/SiO$_2$-300 catalyst showed crystalline RuO$_2$ peaks with (110) plane at 28.1°, (101) at 35.2°, and (211) at 54.5°. All diffraction patterns of the RuNPs/SiO$_2$-300R catalyst showed the metallic ruthenium peaks without any RuO$_2$ planes, and these patterns confirmed that the high-pressure reduction procedure under pure hydrogen gas effectively reduced RuO$_2$ to metallic Ru.

Table I. Textural properties of the synthesized ruthenium nanoparticle-embedded silica (RuNPs/SiO$_2$) catalysts.

Catalyst	BET surface area (m^2/g)	Pore volume (cm^3/g)	BJH pore size (nm)
RuNPs/SiO$_2$-D	45.2	0.138	12.2
RuNPs/SiO$_2$-300	878.6	0.969	4.52
RuNPs/SiO$_2$-300R	783.9	0.885	4.41
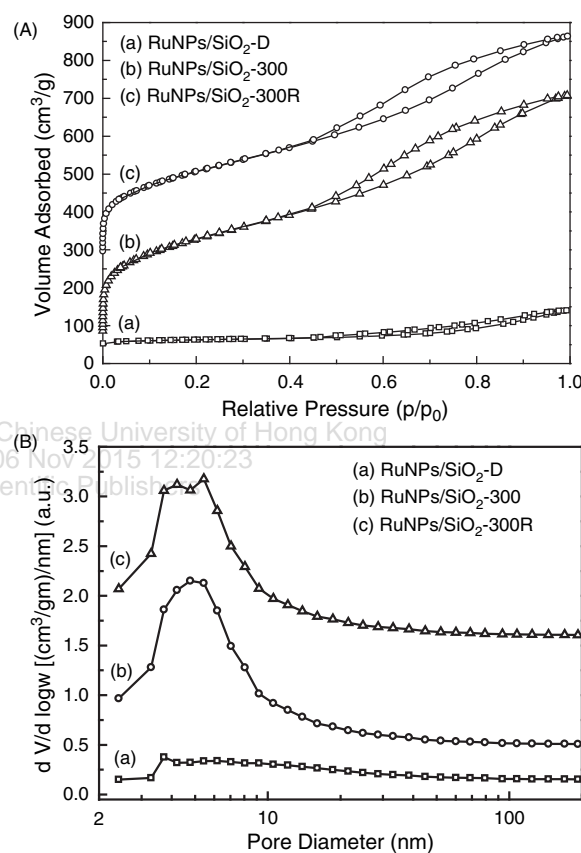
Fig. 3. Nitrogen adsorption–desorption isotherms (left) and pore size distributions (right) of the synthesized RuNPs/SiO$_2$ catalysts. (a) RuNPs/SiO$_2$-D, (b) RuNPs/SiO$_2$-300, and (c) RuNPs/SiO$_2$-300R.

Figure 6 shows the molar concentrations of SAN and GBL as a function of reaction time at different reaction temperatures using the RuNPs/SiO$_2$-300R catalyst for the hydrogenation of SAN. At a reaction temperature of 423 K, SAN was slowly converted to GBL, but at the higher temperatures of 458 K and 473 K, the 90% conversion of SAN was achieved in a reaction time of approximately 2 and 3 h, respectively. After 6 h at a reaction temperature of 473 K, 98% of SAN was converted. The maximum yield of GBL from the hydrogenation of SAN using the RuNPs/SiO$_2$-300R catalyst was 90.1% (reaction
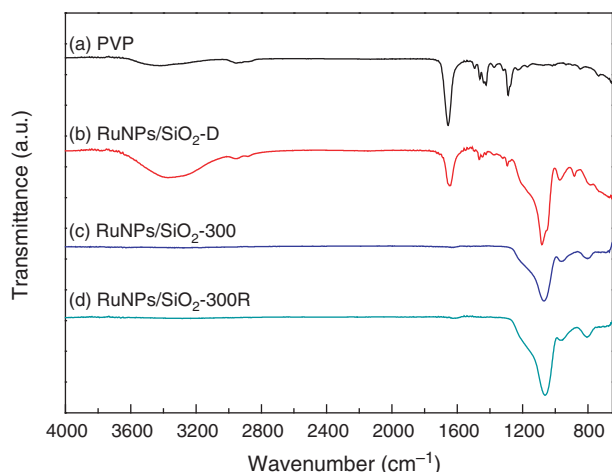
Fig. 4. FT-IR spectra of synthesized RuNPs/SiO$_2$ catalysts. (a) PVP, (b) RuNPs/SiO$_2$-D, (c) RuNPs/SiO$_2$-300, and (d) RuNPs/SiO$_2$-300R.
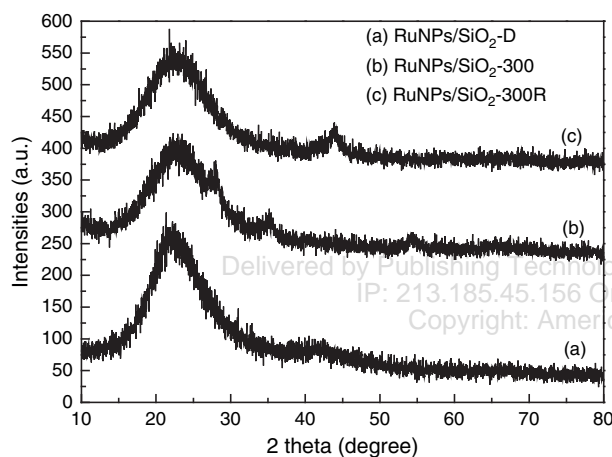
Fig. 5. Powder X-ray diffraction patterns of the synthesized RuNPs/SiO$_2$ catalysts. (a) RuNPs/SiO$_2$-D, (b) RuNPs/SiO$_2$-300, and (c) RuNPs/SiO$_2$-300R.
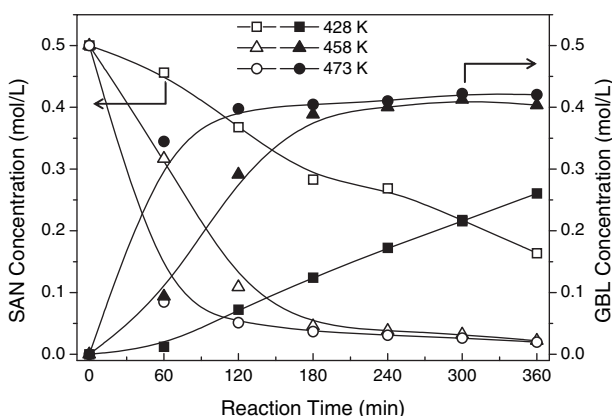
Fig. 6. Molar concentrations of succinic anhydride (SAN, open symbol) and γ-butyrolactone (GBL, solid symbol) as functions of reaction time during the hydrogenation of SAN. Reaction conditions: 0.5 mol/L of succinic anhydride; 50 mL of 1,4-dioxane; 0.3 g of RuNPs/SiO$_2$-300R catalyst; 50 bar H$_2$; stirring rate: 750 rpm.
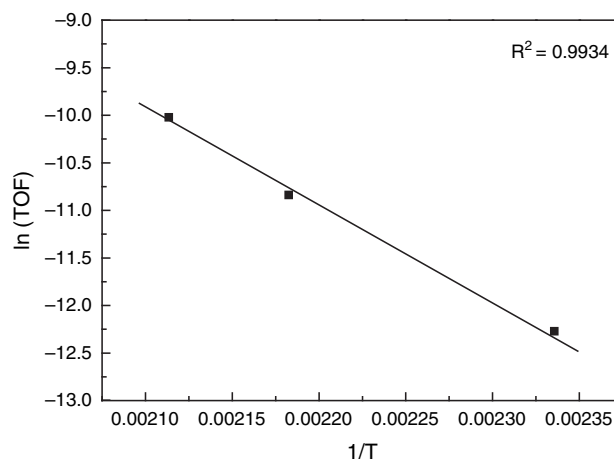
Fig. 7. Arrhenius plot for the calculation of observed activation energy for the hydrogenation of succinic anhydride over the RuNPs/SiO$_2$-300R catalyst. The slope of this graph ($-E_{a,obs}/R$) was obtained from the TOF values based on the observed initial reaction rate.

conditions: 473 K at 5 h), however, after 5 h, the yield of GBL slightly decreased because it was further converted into 1,4-butanediol, butanoic acid, 1-butanol, and ethanol, which was confirmed by GC-MS analysis. The observed activation energy ($E_{a,obs}$) was obtained from the TOF values at the different reaction temperatures (the dispersion of RuNPs was calculated assuming the presence of spherical nanoparticles with $D = 1.33/d$, where D is dispersion and d is the average particle size), shown in Figure 7.[36, 37] When the liquid-phase reactions were conducted without mass transfer limitation, the rate of the reactions was strongly affected by the reaction temperature, and the observed activation energy of above 40 kJ/mol suggest that the reaction was not controlled by mass transfer.[38, 39] The value of $E_{a,obs}$ in this study was 83.1 kJ/mol, and this sufficiently large value of $E_{a,obs}$ suggested that the activity measurement was conducted in the kinetic region (the free region of mass transfer).

4. CONCLUSIONS

The application of synthesized metal nanoparticles to heterogeneous catalysis has been of interest, but metal nanoparticles have not yet been fully applied because of their incompatibility with high-pressure and high-temperature reactions. In this study, we synthesized a catalyst consisting of highly dispersed ruthenium nanoparticles embedded in mesoporous silica (RuNPs/SiO$_2$), which was utilized in the conversion of SAN to GBL via liquid-phase hydrogenation. In the preparation of the RuNPs/SiO$_2$ catalyst, thermal treatment of the synthesized RuNPs/SiO$_2$-D was necessary to produce the mesoporous textural properties of the silica support material. Coordinated carbonyl groups of PVP remaining from the synthesis of the RuNPs were effectively removed by the elimination of PVP by

thermal treatment. After the thermal treatment, the size and shape of the embedded RuNPs were nearly unchanged, and the catalyst was active in the hydrogenation of SAN to produce GBL with a maximum yield of 90.1%.

References and Notes

1. G. C. Bond, *Chem. Soc. Rev.* 20, 441 (**1991**).
2. R. A. Santen, *Acc. Chem. Res.* 42, 57 (**2009**).
3. G. A. Somorjai, H. Frei, and J. Y. Park, *J. Am. Chem. Soc.* 131, 16589 (**2009**).
4. M. Haruta, S. Tsubota, T. Kobayashi, H. Kageyama, M. J. Genet, and B. J. Delmon, *J. Catal.* 144, 175 (**1993**).
5. B. Niu, W. Xu, Z. Guo, N. Zhou, Y. Liu, Z. Shi, and Y. Lian, *J. Nanosci. Nanotechnol.* 12, 7376 (**2012**).
6. D. W. Zhang, C. Chen, J. Zhang, and F. Ren, *J. Mater. Sci.* 43, 1492 (**2008**).
7. A. Jung, S. Cho, W. J. Cho, and K.-H. Lee, *Korean J. Chem. Eng.* 29, 243 (**2012**).
8. S. Jung and J. H. Kim, *Korean J. Chem. Eng.* 27, 645 (**2010**).
9. S. Sun, C. B. Muarry, D. Weller, L. Folks, and A. Mosre, *Science* 287, 1989 (**2000**).
10. R. J. Joseyphus, T. Matsumoto, H. Takahashi, D. Kodama, K. Tohji, and B. Jeyadevan, *J. Solid State Chem.* 180, 3008 (**2007**).
11. G. W. Qin, W. L. Pei, Y. P. Ren, Y. Shimada, Y. Endo, M. Yamaguchi, S. Okamoto, and O. Kitakami, *J. Nanosci. Nanotechnol.* 11, 10796 (**2011**).
12. J.-S. Lim, D.-H. Kim, V. Mathew, D.-C. Ahn, and J.-K. Kim, *J. Nanosci. Nanotechnol.* 11, 1451 (**2011**).
13. J. Sui, C. Zhang, J. Li, and W. Cai, *J. Nanosci. Nanotechnol.* 12, 3867 (**2012**).
14. S. H. Joo, J. Y. Park, J. R. Renzas, D. R. Butcher, W. Huang, and G. A. Somorjai, *Nano Lett.* 10, 2709 (**2010**).
15. I. Lee, F. Delbecq, R. Morales, M. A. Albiter, and F. Zaera, *Nat. Mater.* 8, 132 (**2009**).
16. V. Karel, H. Kim, A. D. Stump, A. B. Schult, M. J. H.-Smith, C. Edwards, A. R. James, J. Caruso, T. T. Kodas, S. T. Haubrich, and M. H. Kowalski, US Patent 7575621 (**2009**).
17. Y. H. Kim, J. E. Park, H. C. Lee, S. H. Choi, and E. D. Park, *Appl. Catal. B: Environ.* 127, 129 (**2012**).
18. C. J. H. Jacobsen, S. Dahl, P. L. Hansen, E. Tornqvist, L. Jensen, H. Topsoe, D. V. Prip, P. B. moenshaug, and I. Chorkendorff, *J. Mol. Catal. A: Chem.* 163, 19 (**2000**).
19. B. Lee, I.H. Jang, J. W. Bae, S. H. Um, P. J. Yoo, M.-J. Park, Y. C. Lee, and K.-W. Jun, *Catal. Surv. Asia*, 16, 121 (**2012**).
20. V. M. Deshpande, K. Ramanarayan, and C. S. Narasimhan, *J. Catal.* 121, 174 (**1990**).
21. J. Struijk, M. d'Angremond, W. J. M. Lucas-de Regt, and J. J. F. Scholten, *Appl. Catal. A: Gen.* 83, 263 (**1992**).
22. B. Zuo, Y. Wang, Q. Wang, J. Zhang, N. Wu, L. Peng, L. Gui, X. Wang, R. Wang, and D. Yu, *J. Catal.* 222, 493 (**2004**).
23. Y. Hara, H. Kusaka, H. Inagaki, K. Takahashi, and K. Wada, *J. Catal.* 194, 188 (**2000**).
24. A. Takagaki, S. Nishimura, and K. Ebitani, *Catal. Surv. Asia* 16, 164 (**2012**).
25. W. Mesch, and A. Wittwer, US Patent 3957830 (**1976**).
26. U. Herrmann and G. Emig, *Ind. Eng. Chem. Res.* 36, 2885 (**1997**).
27. E. Reale, A. Leyva, A. Corma, C. Martinez, H. Garcia, and F. Rey, *J. Mater. Chem.* 15, 1742 (**2005**).
28. S.-H. Chung, Y.-M. Park, M.-S. Kim, and K.-Y. Lee, Catal. *Today* 185, 205 (**2012**).
29. S. Park, T. J. Kim, Y. M. Chung, S. H. Oh, and I. K. Song, *Korean J. Chem. Eng.* 28, 1359 (**2011**).
30. L. Yang, J. B. Joo, N. D. Kim, K. S. Jung, and J. Yi, *Korean J. Chem. Eng.* 27, 1695 (**2010**).
31. K.-S. Chou and C.-C. Chen, *Micropor. Mesopor. Mat.* 98, 208 (**2007**).
32. K.-T. Li, M.-H. Hsu, and I. Wang, *Catal. Commun.* 9, 2257 (**2008**).
33. H. Lee, S. Kim, D.-W. Lee, and K.-Y. Lee, *Catal. Commun.* 12, 968 (**2011**).
34. A. Nemancha, H. Moumeni, and J. L. Rehspringer, *Physics Procedia* 2, 713 (**2009**).
35. J. A. L.-Sanchez, N. Dimitratos, C. Hammond, G. L. Brett, L. Kesavan, S. White, P. Miedziak, R. Tiruvalam, R. L. Jenkins, A. F. Carley, D. Knight, C. J. Kiely, and G. J. Hutchings, *Nat. Chem.* 3, 551 (**2011**).
36. B. B.-Baeza, A. G.-Ruiz, and I. R.-Ramos, *J. Catal.* 229, 439 (**2005**).
37. M. L. Toebes, F. F. Prinsloo, J. H. Bitter, A. J. Dillen, and K. P. Jong, *J. Catal.* 214, 78 (**2003**).
38. R. L. Augustine, Heterogeneous Catalysis for the Synthetic Chemist, Dekker, New York (**1995**).
39. J. Hajek and D. Y. Murzin, *Ind. Eng. Chem. Res.* 43, 2030 (**2004**).